ACS Biomaterials SCIENCE & ENGINEERING

Article

pubs.acs.org/journal/abseba

Collagen Fibril Response to Strain in Scaffolds from Ovine Forestomach for Tissue Engineering

Katie H. Sizeland,[†,‡] Hannah C. Wells,[†] Susyn J.R. Kelly,[†] Keira E. Nesdale,[†] Barnaby C. H. May,[§] Sandi G. Dempsey,[§] Christopher H. Miller,[§] Nigel Kirby,[‡] Adrian Hawley,[‡] Stephen Mudie,[‡] Tim Ryan,[‡] David Cookson,[‡] and Richard G. Haverkamp*[,†]

[†]School of Engineering and Advanced Technology, Massey University, Palmerston North 4472, New Zealand

[‡]Australian Synchrotron, 800 Blackburn Road, Clayton, Melbourne, Victoria 3168, Australia

[§]Aroa Biosurgery, 2 Kingsford Smith Place, Airport Oaks, Auckland 2022, New Zealand

ABSTRACT: Scaffold biomaterials are typically applied surgically as reinforcement for weakened or damaged tissue, acting as substrates on which healing tissue can grow. Natural extracellular matrix (ECM) materials consisting mainly of collagen are often used for this purpose, but are anisotropic. Ovine forestomach matrix (OFM) ECM was exposed to increasing strain and synchrotron-based SAXS diffraction patterns and revealed that the collagen fibrils within underwent changes in orientation, orientation index (a measure of isotropy), and extension. Response to the strain depended on the direction the collagen fibrils were oriented. When the ECM was stretched in the direction of collagen fibril orientation, the fibrils become more oriented and begin to take up the strain immediately (as shown by the increased *d*-spacing). Stretch applied perpendicular to dominant fibril direction caused the fibrils to initially become less oriented as they were pulled away from the original direction, and less force was initially transmitted along the length of the fibrils (i.e., the *d*-spacing changed less). SAXS analysis of OFM and the starting raw tissue showed there is no difference in the structural arrangement of the collagen fibrils. Understanding the directional structural response of these materials under strain may influence how surgeons select and place the materials in use.

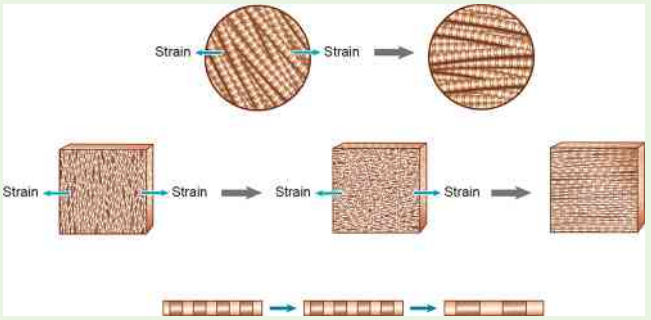

KEYWORDS: *collagen, scaffold, small-angle X-ray scattering, orientation, differential scanning calorimetry, scanning electron microscopy*

1. INTRODUCTION

Because many injuries are unable to heal, surgeons use scaffold materials to replace or repair damaged tissues, or to support their regeneration. Successful constructive remodeling and repair of tissues has been facilitated by the development of extracellular matrix (ECM) scaffold materials and their use preclinically and clinically.[1] A large range of scaffolds, including ECM materials, are commercially available for internal tissue engineering and for dermal reconstruction.[2−4] It is vital that the physical properties of the material selected for use render it able to withstand the strains to which it will be subject in situ. Common clinical applications include: abdominal hernia repair,[5] providing support during breast reconstruction,[6] rotator cuff repair,[7] tendon repair,[8] and substituting for skin in serious burns and chronic wounds.[9]

Surgeons can choose to use either synthetic or natural scaffolds. Synthetic scaffolds include absorbable, nonresorbable, or composite materials.[10−12] Natural allograft or xenograft scaffolds have been developed, derived from the ECM of a number of different human and animal tissues. Ovine forestomach scaffolds,[13] porcine dermis xenografts,[14] and human dermis allografts[15] have been evaluated, in both preclinical and clinical models of tissue regeneration. Tissue-engineered vascular grafts have also been investigated.[16] Clinically, porcine-derived bladder matrices have been successfully integrated, thereby repairing a host's tympanic membrane in one study[17] and a bladder in another.[18] Scaffolds of small intestinal submucosa were used as small-diameter arterial grafts for dogs,[19] and use of equine pericardium resulted in the healing of difficult-to-close to wounds.[20]

Collagen-based materials are highly suitable as surgical scaffolds because of their excellent biocompatibility[21] once they have been thoroughly decellularized. Furthermore, they provide high mechanical strength, or toughness, because of the structure of the tissues from which they are derived. These tissues are elastic and can resist tearing owing to the inherent strength and elasticity of the collagen fibrils they are made of[22] and the ability of those fibrils to be rearranged and block a

Received: August 16, 2017
Accepted: August 28, 2017
Published: August 28, 2017

DOI: 10.1021/acsbiomaterials.7b00588
ACS Biomater. Sci. Eng. XXXX, XXX, XXX−XXX

propagating tear.[23] Natural collagen tissues are sufficiently porous for cells to infiltrate and populate the implanted scaffolds.[24] With time, collagen scaffolds are remodeled and absorbed and eventually replaced by the patient's own tissue.[25] This combination of factors gives native, structured, collagen-based materials clear advantages over their alternatives.

The relationships between the structural and mechanical properties of scaffolds derived from bovine, porcine, ovine, and human sources have been characterized.[26,27] Ovine forestomach matrix (OFM) scaffolds have shown to retain their native collagen *d*-spacing and can be laminated to generate multiply biomaterials suitable for clinical applications where the resultant device will be placed under load.[27] Acellular porcine grafts from small intestine submucosa, the pericardium, and dermal sources were compared and scaffolds from the small intestine submucosa proved to be the strongest.[28] An interspecies comparison found that the biocompatibility of human acellular dermal matrix (ADM) and porcine ADM was very similar.[29] A different study, which included bovine ADM with the others, yielded no uniform relationship between fibril orientation and strength in the three tissues.[26] The human and bovine scaffolds were isotropic, whereas the porcine scaffold was anisotropic. In terms of strength, porcine was the weakest and bovine was the strongest scaffold, with stronger materials having a more layered structure.[26] Collagen fibril reorientation when the biomaterial was under biaxial strain was shown to cause increased stiffness upon drying,[30] and the volume of individual collagen fibrils was shown to decrease with increasing strain (reflected in a high Poisson ratio).[22]

Small-angle X-ray scattering (SAXS) can provide detailed information on the architecture of collagen materials, including fibril orientation and *d*-spacing.[26,31−34] Tissue strength is correlated with the orientation of collagen fibrils in skin, measured edge-on (i.e., alignment in-plane), across a range of mammal species.[35−37] In turn, fibril orientation (and *d*-spacing) appears to be affected by the hydration of a skin while it is being processed to leather.[38] The addition of penetrating oils or fatliquors during the processing increased the *d*-spacing but no correlation was found between the amount of fatliquor used and the structural response of the material to strain.[39,40]

Here, we investigate the structure of a commercially available ECM scaffold derived from ovine forestomach to better understand how the material's biomechanical properties are influenced by the architecture of its collagen, and make comparisons between the finished biomaterial and the starting raw material.

2. EXPERIMENTAL METHODS

2.1. Test Materials. Commercially available, terminally sterilized (ethylene oxide) ovine forestomach matrix (OFM), was supplied by Aroa Biosurgery. Ovine forestomach tissue (OFT), the raw material used to produce OFM, was prepared from intact ovine forestomach via separation of the tissue ECM from the muscle layer.[13] The epithelial layer was removed to reduce any interference from the keratinized squamous epithelial layer on the thermal stability of the collagen analysis. This was manually removed following incubation of the tissue with mild detergent (Tx-100) and chelating agent (EDTA). Promogran, a terminally sterilized (γ radiation) collagen wound dressing was manufactured by Systagenix, (product code: PG004, lot number: 1605/4/1/3)). All tests (except scanning electron microscopy) were done on samples that had first been fully hydrated.

2.2. Scanning Electron Microscopy (SEM). Samples of OFM were cut into small cubes and fixed in modified Karnovsky's fixative (3% glutaraldehyde and 2% formaldehyde in 0.1 M phosphate buffer; pH 7.2) for over 8 h at room temperature. After being washed three times for 10−15 min each time in 0.1 M phosphate buffer (pH 7.2), the samples were dehydrated using a graded series of ethanol washes (25, 75, 95, 100%), with each ethanol wash being 10−15 min long. A final 100% ethanol wash for 1 h followed. Samples were critical point (CP) dried using the Polaron E3000 series II apparatus with liquid CO_2 as the CP fluid and 100% ethanol as the intermediary fluid. The samples were then mounted on aluminum stubs and coated with gold using a Baltec SCD 050 sputter coater. A FEI Quanta 200 environmental scanning electron microscope was used to view the samples at an accelerating voltage of 20 kV.

2.3. Sirius Red Staining. Samples were hydrated in phosphate buffered saline (pH 7.4) for 60 min and then fixed in 10% neutral buffered formalin (Sigma-Aldrich) for 24 h. Fixed samples were processed using standard histological techniques; briefly, samples were dehydrated in a series of ethanol, and then embedded in paraffin blocks. Blocks were cut into 10 μm thick sections and placed on slides to dry. Slides were deparaffinized and hydrated before staining for 60 min in a solution of Sirius Red (F3B (Sigma-Aldrich) as a 0.1% (w/v) in saturated aqueous picric acid. Slides were then washed twice in acidified water, dehydrated, cleared with xylene, and mounted under coverslips. Slides were imaged using a Leica DMR upright microscope with polarized light and a Nikon Digital Sight camera using Nikon NIS Elements for image acquisition.

2.4. Differential Scanning Calorimetry (DSC). Samples were hydrated in phosphate buffered saline (pH 7.4) for approximately 5 min then cut to a final mass of 5 to 20 mg. Samples were placed flat in a Tzero Analysis pan (TA, Switzerland) and sealed with a hermetic lid. DSC measurements used a TA Instruments Q20 (DE, USA) with a temperature ramp program which included an equilibration step to 10 °C (30 min) and a ramp of 8 °C/min to 120 °C. Linear sections of the curve on either side of the thermal event peak were selected to calculate the onset temperature, peak temperature, and enthalpy.

2.5. Small-Angle X-ray Scattering. Diffraction patterns were recorded for the samples on the SAXS/WAXS beamline at the Australian Synchrotron using a high-intensity undulator source with an energy resolution of 1×10^{-4} from a cryo-cooled Si (111) double-crystal monochromator. The beam size (fwhm focused at the sample) was 250×80 μm with a total photon flux of about 2×10^{12} ph s^{-1}. All diffraction patterns were recorded with an X-ray energy of 12 keV using a Pilatus 1 M detector with an active area of 170×170 mm and a sample-to-detector distance of 3371 mm. Exposure time for diffraction patterns was 1 s. Data was processed using the Scatterbrain analysis software.

Squares of about 5×5 mm of OFM and OFT were prepared and mounted with the surface perpendicular to the X-ray beam and scattering patterns recorded with the samples under no strain.

For measuring the samples under strain, strips of the OFM (1×30 mm) were cut and mounted such that the surface would be exposed to the X-ray beam flat-on or perpendicular. Strips were cut at 90 deg to one another to obtain structural information in two directions (see below). A stretching apparatus similar to that described in[36] was used with custom built roller grips having scored and opposing surfaces to ensure the samples remained firmly in place when increasing amounts of tension were applied. Samples were mounted horizontally without tension or slack between the jaws of the stretching machine (Figure 1). Samples were rehydrated with water before they were placed in the beamline and were kept hydrated throughout the full measurements period. Initial force and extension was recorded and then the sample was stretched by 1 mm, maintained at this extension for 1 min, and then diffraction patterns recorded. Force and extension were again recorded. This process was repeated until the sample failed.Orientation direction is the average direction of the collagen fibrils and is determined from an azimuthal angle-versus-intensity plot; it is the central position of a Gaussian peak fitted to the smallest azimuthal angle range that contains 50% of the fibrils.

Orientation index (OI) is defined as $(90° - OA)/90°$, where OA is the azimuthal angle range that contains 50% of the fibrils centered at the orientation direction. The OI provides a measure of the spread in orientation of the fibrils where an OI of 0 indicates the fibrils are

DOI: 10.1021/acsbiomaterials.7b00588
ACS Biomater. Sci. Eng. XXXX, XXX, XXX−XXX

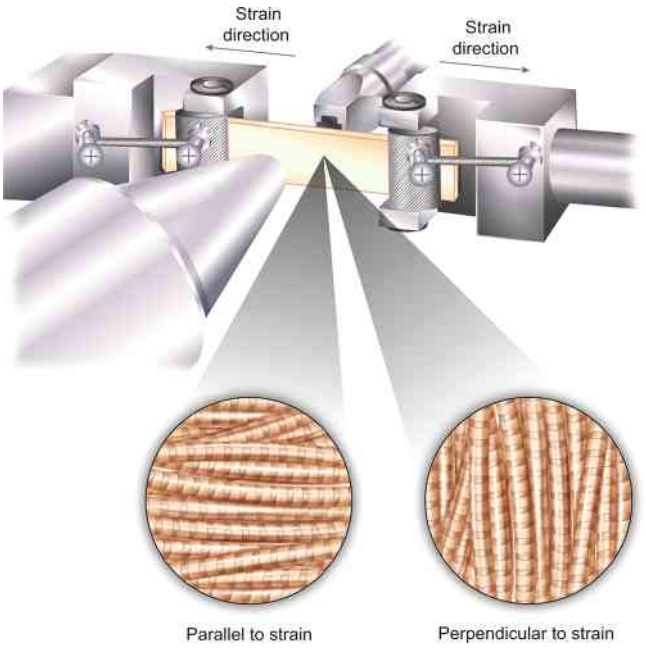

Figure 1. Experimental setup for SAXS analysis of samples under strain.

completely randomly oriented and an OI of 1 indicates the fibrils are completely parallel to each other. The OI is calculated at the most intense *d*-spacing peak which, in this case, was the fifth order peak, around 0.059−0.060 $Å^{-1}$.

The *d*-spacing was determined from Bragg's Law by taking the center of a Gaussian curve fitted to the sixth order diffraction peak of an integrated intensity plot for each spectrum.

2.6. SAXS before and during Strain. To assess the effect of collagen fibril direction on the response of the material to strain, samples with the collagen fibrils approximately parallel to the direction of strain, and with the collagen fibrils at a large angle away from the direction of strain were measured. Twenty strips of material were examined with SAXS, the collagen fibril orientation index (OI, the spread of fibril direction; see below) and orientation direction determined and suitable candidates were selected from these (Table 1).

For each sample of OFM, nine diffraction patterns were recorded in a small grid (1 × 1 mm) that was positioned at the center of the sample (which moved after each incremental increase of strain). The nine measurements of each of OI and *d*-spacing were then averaged. The spread in these values gave the estimate of errors.

2.7. Elastic Modulus Measurement. Stress−strain curves were measured during the SAXS measurements on strained materials. A load cell recorded the applied stress to the horizontally mounted samples. The time between each increment of strain was 3−4 min. The elastic modulus was calculated from these measurements using the full range of applied strain.

3. RESULTS

3.1. SEM of Ovine Forestomach Matrix (OFM). Ovine forestomach matrix had an open structure, with regions of fairly well oriented fibers (Figure 2). Both the top and bottom surfaces appeared to be porous and this porosity extended throughout the thickness of the material.

3.2. Sirius Red Staining. Sirius Red-stained sections of OFT, OFM, and Promogran demonstrate birefringence (red and green) from collagen fibers when imaged with cross-polarized light (Figure 3). Thicker samples give a red color and thinner samples green. These reveal some differences in fiber size for each sample type.

Table 1. Orientation Index and Orientation Direction of Fibrils in OFM Samples Measured Prior to Further Strain Measurements[a]

sample name	orientation index (OI)	orientation direction (° from long axis)
OFM1	0.33	−35
OFM2	0.41	−27
OFM3	0.44	18
OFM4	0.28	−65
OFM5	0.53	25
OFM6	*0.63*	*−58*
OFM7	**0.61**	**15**
OFM8	0.55	−30
OFM11	0.58	12
OFM12	*0.75*	*−45*
OFM13	0.74	−58
OFM14	**0.46**	**13**
OFM15	0.55	−30
OFM16	0.23	17
OFM17	0.22	58
OFM18	0.61	−42
OFM19	0.35	72
OFM23	0.39	−50
OFM25	0.55	3
OFM26	0.60	−28

[a]Bold lines, samples selected with fibrils oriented close to the strain direction; italic lines, samples selected with fibrils at a significant angle to strain direction.

3.3. DSC of OFT and OFM. Average DSC melting temperature for OFT was 65.4 °C (σ = 0.8, n = 30) and for OFM 61.1 °C (σ = 3.5, n = 30). Although the difference in the melt onset temperatures of the two samples is statistically significant (t test for different means gives $P < 0.001$) the difference is small. As a comparison a reconstituted collagen material (using Promogran as a representative material) gave a melt onset temperature of 27.9 °C (σ = 0.3, n = 30) (Figure 4).

3.4. OI and *d*-Spacing of OFT and OFM. The OI of the OFT was 0.302 (σ = 0.125, n = 55) compared with the OI of OFM of 0.315 (σ = 0.137, n = 26). A t test for equal means gave p = 0.24) therefore the difference in the mean values is not great enough to reject the possibility that the difference is due to random sampling variability. There is not a statistically significant difference in the structural arrangement of the collagen fibrils by this measure. For the *d*-spacing, the OFT gave d = 64.77 nm (σ = 0.12, n = 55) and OFM gave d= 64.34 nm (σ = 0.13, n = 26) nm and this difference is statistically significant (the t test for equal means gives $p < 0.001$). *d*-Spacing is affected by water (larger when wet) and by fats and oils[39] so the slightly higher *d*-spacing for OFT could be becauseit contained a little fat or that it was slightly better hydrated.

3.5. SAXS before and during Strain. The collagen fibril orientation index (OI, the spread of fibril direction; see below) and orientation direction determined for a series of OFM samples are listed in Table 1. From these samples, suitable candidates for stretching were selected (shaded in gray, Table 1) based on samples with a high OI and an orientation direction either close to parallel or close to perpendicular to the direction they would be strained. The high OI is selected because the effect of a dominant fibril direction should be more pronounced than in a sample tending to be more isotropic.

DOI: 10.1021/acsbiomaterials.7b00588
ACS Biomater. Sci. Eng. XXXX, XXX, XXX−XXX

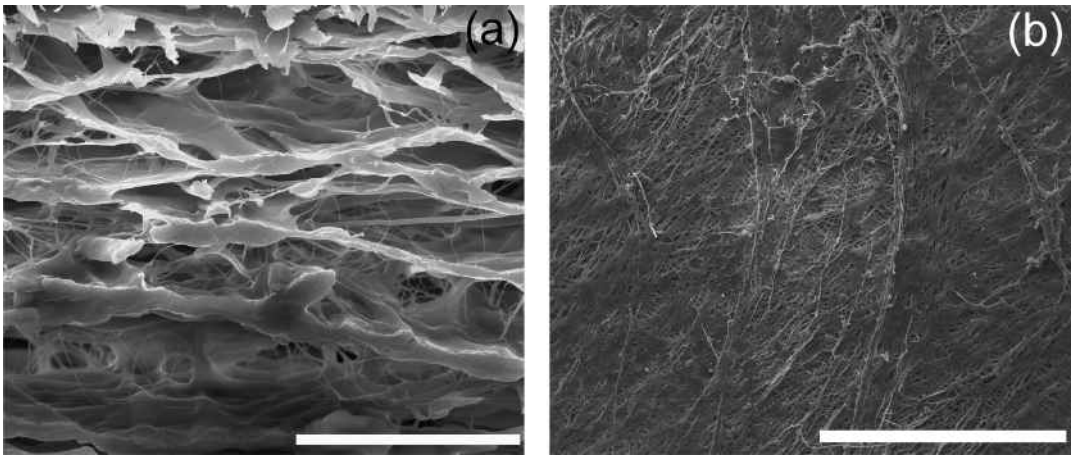

Figure 2. SEM images of OFM (a) edge on; (b) abluminal surface. Scale bars: (a) 40 μm; (b) 1 mm.

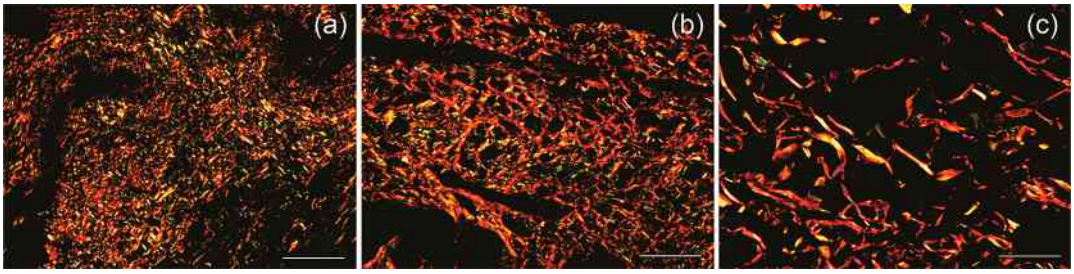

Figure 3. Sirius Red-stained sections of (a) OFT, (b) OFM, and (c) Promogran (scale bars 100 μm).

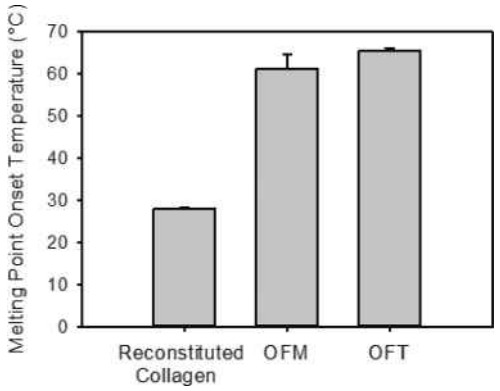

Figure 4. DSC measurements of thermal stability of collagen materials. Error bars represent one standard deviation.

The X-ray scattering patterns recorded for the OFM showed clear diffraction rings due to the axial periodicity of the collagen fibrils (Figure 5). Also apparent in the raw patterns were fibril orientation and OI. Figure 5a shows a representative diffraction pattern of an unstrained sample, where the collagen fibrils are not highly oriented and are approximately parallel (−15°) to the direction the strain will be applied. When strain was applied, (Figure 5b), the pattern rotated slightly to be oriented in the direction of strain and became distorted, reflecting the increase in OI (loss of isotropy). Similarly, an OFM material with the collagen fibrils oriented at a larger angle (55°) to the direction of the strain (Figure 5c) changes such that during strain the orientation direction rotates significantly to be in line with the direction of strain, and OI increases (Figure 5d).

3.6. Orientation and Orientation Index. These changes in OI and orientation are more readily observed in a plot of the variation in scattering intensity with changing azimuthal angle, as shown in Figure 6. The central peaks in Figure 6 coincide with the average collagen fibril direction relative to the SAXS detector, where 0° is horizontal (in this experiment, because the samples were mounted as horizontal strips, 0° represents the direction along the length of the sample). The width of this peak indicates fibril direction spread, with a broader peak corresponding to a wider range of orientations (a lower OI). Orientation shifts toward the direction of applied strain (i.e., 0°) as strain increases (Figure 6). When the collagen is already aligned approximately in the direction of the applied force, this shift was small (Figure 6a), but where the initial direction was very different to the direction of applied strain, this shift was large (Figure 6b). A peak's width also changed, with a narrower peak (larger OI) at the maximum strain (Figure 6).

3.7. Change in D-spacing. The stretch of individual collagen fibrils with increasing strain is apparent as rings in the diffraction patterns (Figure 5), which correspond to an increases in d-spacing visible in any of the diffraction peaks. Integrated intensity plots (Figure 7) show these diffraction peaks from which the D-spacing of the fibrils is measured more clearly. As the OFM is strained, the collagen fibrils are strained, which results in a shift of the diffraction peaks to lower q (larger distance) and some broadening of the peaks, as individual fibrils experience different strain (Figure 7).

3.8. Stress−Strain Curves. Stress−strain curves of OFM samples under strain reveal clear differences between samples with fibrils aligned parallel or perpendicular to the strain (Figure 8a). The material with collagen fibrils oriented in the same direction as the strain shows a higher elastic modulus (0.19−0.22 MPa) than the material with the fibrils initially perpendicular to the strain (0.17−0.13 MPa). Most of this difference is due to the difference in the length of the "toe"

DOI: 10.1021/acsbiomaterials.7b00588
ACS Biomater. Sci. Eng. XXXX, XXX, XXX−XXX

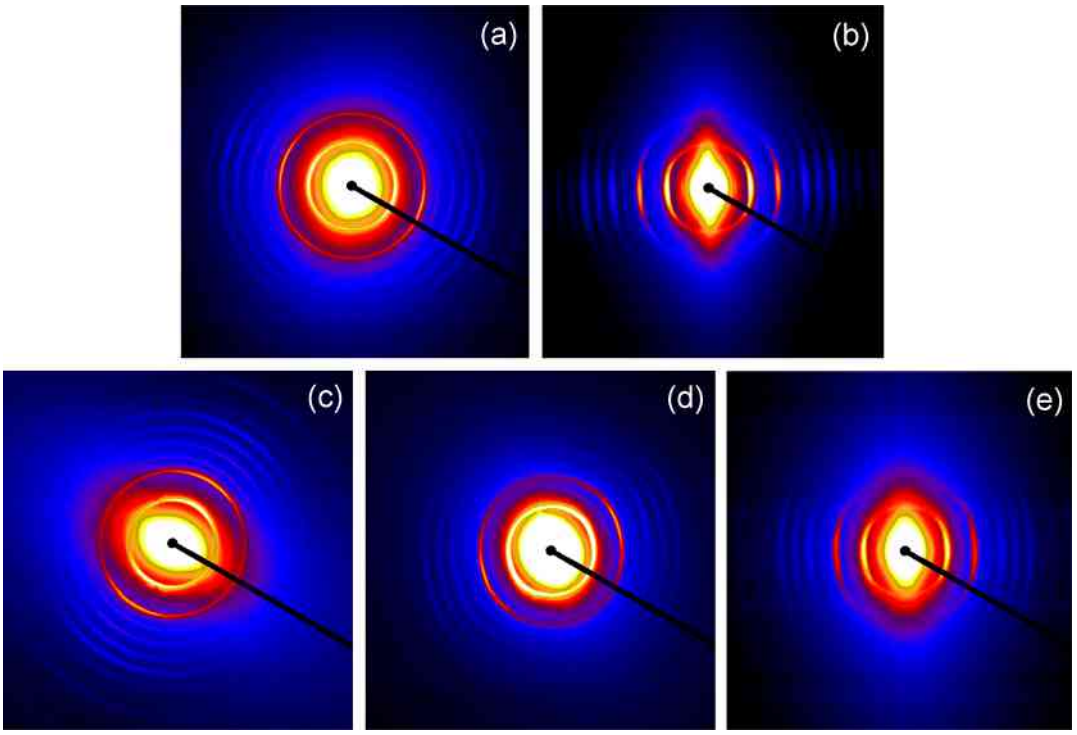

Figure 5. SAXS patterns of OFM. Fibrils initially approximately parallel (−15°) to the stretching direction (a) before strain, (b) during strain prior to failure; fibrils initially at 55° to the stretching direction (c) before strain, (d) during intermediate strain, and (e) during strain prior to failure.

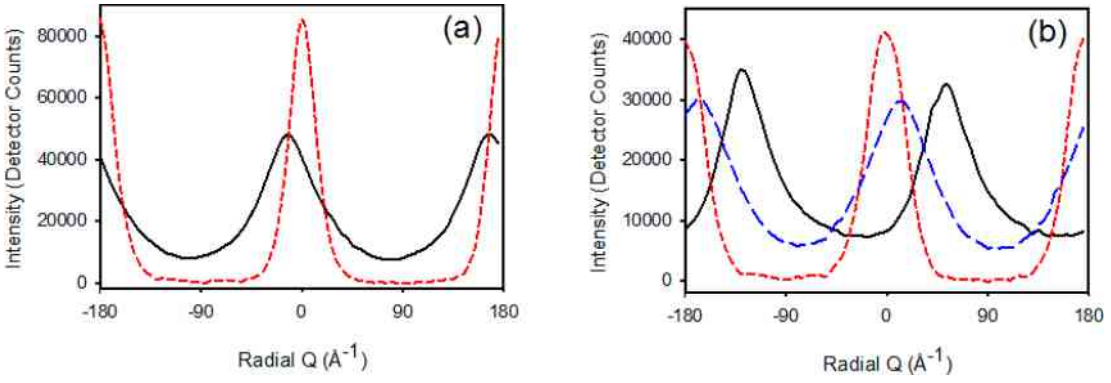

Figure 6. Intensity variation with azimuthal angle for the 5th order diffraction peak of OFM scaffolds (black, before strain; blue, at intermediate strain; red, at maximum strain): (a) with fibrils initially parallel to the stretching direction; (b) with fibrils initially perpendicular to the stretching direction.

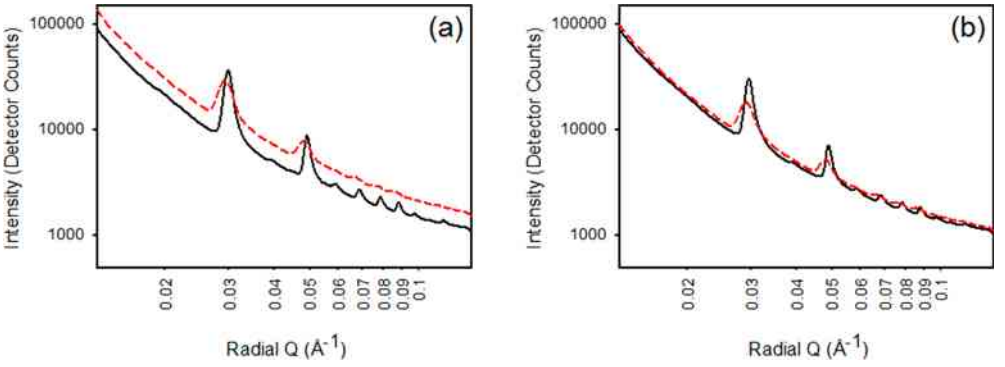

Figure 7. Integrated intensity profile of OFM (black, before strain; red, at maximum strain): (a) with fibrils initially parallel to the stretching direction; (b) with fibrils initially perpendicular to the stretching direction (just one example of each).

DOI: 10.1021/acsbiomaterials.7b00588
ACS Biomater. Sci. Eng. XXXX, XXX, XXX−XXX

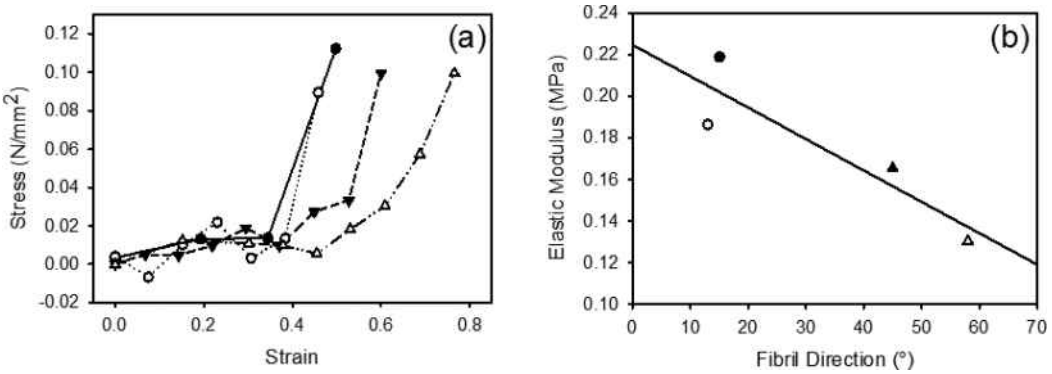

Figure 8. (a) Stress versus strain for two samples with fibrils oriented parallel to the direction of the strain (solid circles, OFT7 15°; open circles, OFT14 13°) and two with fibrils oriented perpendicular to the direction of the strain (solid triangles. OFT12−45°; open triangles, OFT6−58°). (b) Elastic modulus taken from the data in panel a versus initial average fibril direction relative to the strain direction.

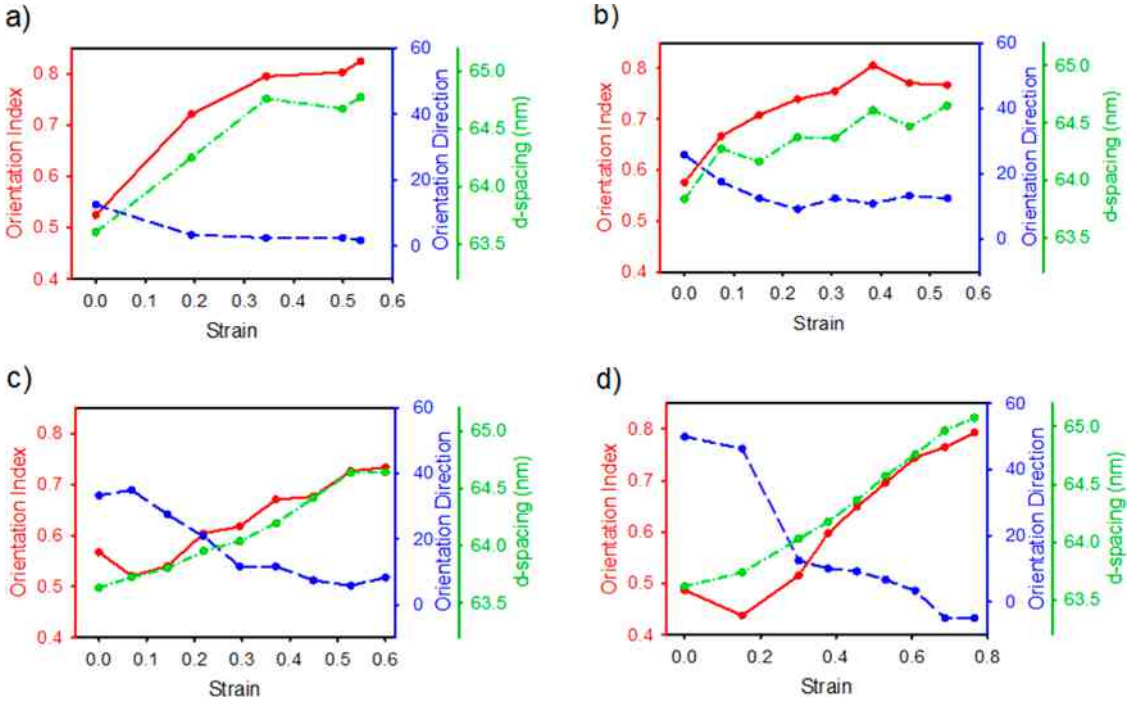

Figure 9. Orientation index (red), orientation direction (blue), and *d*-spacing (green) of samples exposed to increasing strain, with an initial collagen fibril orientation (relative to the direction of strain) of (a) −15, (b) −25, (c) 35, and (d) 55°.

region of the stress strain curve, which is where the reorientation of the collagen fibrils is taking place (Figure 8b). Although the data here is limited, a linear fit to the fibril orientation versus elastic modulus plot gives an r^2 of 0.82, which suggests a correlation may exist.

3.9. SAXS Combined OI, Orientation Direction, and *d*-spacing. To understand the changes taking place in OFM under strain, the changes in three parameters have been plotted: orientation direction, OI, and *d*-spacing (Figure 9). Data from two samples where the initial collagen fibril direction is close to the direction of strain are plotted (Figure 9a starting at −15° and Figure 9b starting at −25°), as are data from two samples where the initial collagen fibril direction is substantially different to the direction of strain (Figure 9c starting at 35° and Figure 9d starting at 55°).

In all samples, fibril orientation changes to be in parallel with the direction of the applied force. Where the initial fibril orientation is close to the direction of the strain, the OI increases immediately and then plateaued (Figure 9a, b). For samples with fibrils aligned perpendicular to the strain, the OI decreases initially, and then with further strain, the OI increases (Figure 9c, d). The change in *d*-spacing roughly follows the change in OI, with a slower initial increase for samples with fibrils orientated perpendicular to the strain.

4. DISCUSSION

The structural arrangement of collagen fibrils in OFT, measured by SAXS as the OI and D-spacing, is preserved upon processing to OFM. The thermal stability, measured by DSC, is only slightly less in OFM than OFT, indicating that collagen is retained largely intact (in comparison with an example material of reconstituted collagen that had much lower thermal stability).

When the collagen material is strained, the collagen fibrils that make up OFM orient in the direction of applied strain. In this study, the samples were mounted so that the initial

DOI: 10.1021/acsbiomaterials.7b00588
ACS Biomater. Sci. Eng. XXXX, XXX, XXX−XXX

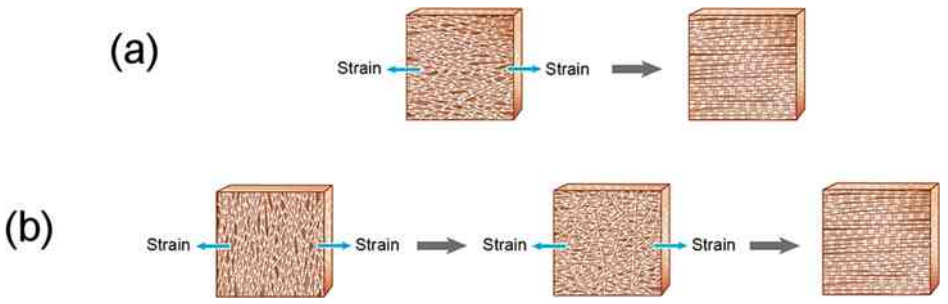

Figure 10. Schematic of change in fibril orientation and OI with increasing strain. (a) When initial fibril orientation is in the direction of strain; (b) when initial fibril orientation is perpendicular to the direction of strain.

orientation varied as much as 55° from the direction of strain or as little at 15° (Figure 9). Regardless, the collagen fibrils became aligned in the direction of strain. This rearranging of fibrils continues over a strain of 0.25−0.30 and eventually results in the fibrils being aligned parallel to the strain direction. It is perhaps unsurprising that a material that consists of fibers should become aligned in the direction of strain, but the ease with, and extent to which this occurs is remarkable. A similar rearranging of collagen fibrils that then blocks the propagation of tearing has been previously identified as a major contributor to the tear resistance of these materials.[23]

Although the collagen fibrils are in the process of aligning to the direction of strain, the OI is also affected. In the simpler case, where the fibrils are already largely oriented in the direction of strain, the OI increases steeply at first with increasing strain and then more gradually (up to a strain of 0.55) before the samples fail. The change in OI is large, going from 0.52−0.80 (Figure 9a) and 0.55−0.82 (Figure 9b).

When the initial orientation direction is not close to the direction of strain, a different change in OI is observed. First the OI decreases, then it increases and continues to increase over the full range of strain before the samples fail (Figure 9c, d). The initial drop in OI is a consequence of the orientation of the fibrils changing to align to the direction of strain. Rotation of the whole tissue could result in OI being constant while fibril orientation changes, but with increasing strain the material is being internally rearranged and passes through an intermediate state in which the fibrils are transitioning from being oriented away from the strain direction to being parallel to the strain direction. This concept is illustrated in Figure 10.

The OI ultimately reached for each sample at maximum strain is similar regardless of initial fibril alignment relative to strain. Clearly, this finding highlights just how effectively fibril orientation can be altered in OFM when the biomaterial is placed under strain.

The *d*-spacing can be likened to an internal stress gauge in the ECM material.[22] When the initial orientation of the collagen fibrils is not close to the direction of strain, the *d*-spacing rapidly climbs with increasing strain, even at the early stages of strain application. In contrast, when the initial fibril orientation is very different to the direction of strain, there is an initial decrease in the *d*-spacing with strain (at about the same stage as the decrease in OI) and then with further strain, the *d*-spacing increases. The difference in the internal strain gauge's response to applied strain can also be related to the fact that when the fibrils are already oriented in the direction of strain, they experience the strain directly, whereas when the fibrils are initially arranged at a large angle from the direction of strain, that strain first prompts a realigning of the fibrils. In this latter instance, only once the fibrils are approximately aligned with the direction of strain do the fibrils extend along with the tissue (Figure 10), which is derived from the changes in SAXS patterns including those shown in Figure 5 and the corresponding azimuthal angle intensity plots shown in Figure 6.

The differences in the elastic behavior of samples cut in different orientations can be explained in terms of the structural arrangement of the collagen fibrils present in the starting tissue. Collagen fibrils provide resistance to strain along their length due to the inherent strength and elasticity of individual fibrils;[22] note that the relatively weak connections between fibrils provide little resistance to strain.[41] When the fibrils are arranged predominantly in the direction of strain, there is only some fibril rearranging before individual collagen fibrils begin to stretch. However, when the fibrils are arranged predominantly away from the direction of applied strain, there is a major rearranging of the fibrils, with the tissue transitioning through a more disorganized state. Consequently, the tissue experiences greater strain before its fibrils become oriented in the direction of strain and can resist to the increasing strain. We can therefore understand and predict the mechanical properties of these tissue based biomaterials based on their collagen structure.

We have shown how the arrangement of the collagen fibrils dictates the physical properties of collagen-based scaffold materials. We have shown that it is possible to measure the arrangement of collagen fibrils and their response to increasing strain. This improved understanding of the structural characteristics and mechanical behaviors of ECM scaffolds can be used to optimize how tissue-engineered products are developed for specific load bearing clinical applications.

5. CONCLUSIONS

Extracellular matrix scaffold materials derived from ovine forestomach have an oriented collagen fibril structure. The structure is minimally changed from the native material by processing. This structure changes as load is applied to the biomaterial. Initially, fibril alignment changes so that fibrils become oriented in the direction of applied strain. However, the fibril response is dependent on the initial orientation of the fibrils relative to the direction of the strain. If a sample's fibrils are already approximately parallel to the direction of the applied strain, fibril orientation gradually changes to match the direction of applied strain; the OI increases consistently until the fibrils become more aligned; and the *d*-spacing immediately reflects the strain (on individual collagen fibrils) that is applied to the sample. When the fibrils are initially aligned at a large angle to the direction of strain, fibril reorientation still occurs to

DOI: 10.1021/acsbiomaterials.7b00588
ACS Biomater. Sci. Eng. XXXX, XXX, XXX−XXX

align the fibers to the direction of the strain via a two-step process. The OI first drops as the OFM structure goes through of transition state from the fibrils being oriented in one direction to being oriented in a different direction before the OI increases as the fibers become aligned with the direction of the applied load. In contrast, the *d*-spacing gradually increases throughout as the strain is released from the fibrils as they become reoriented. The directional structural response of these materials under strain may influence their surgical application.

AUTHOR INFORMATION

Corresponding Author

*E-mail: r.haverkamp@massey.ac.nz. Phone: +64 63569099.

ORCID

Richard G. Haverkamp: 0000-0002-3890-7105

Funding

The Australian Synchrotron provided beamtime and funding for travel and accommodation. Aroa Biosurgery Ltd. provided samples of OFM and OFT and a research grant for this study.

Notes

The authors declare the following competing financial interest(s): B.C.H.M. and C.H.M. are shareholders in Aroa Biosurgery Ltd. S.G.D. is an employee of Aroa Biosurgery Ltd. Aroa Biosurgery Ltd provided a research grant to Massey University to partially fund this study.

ACKNOWLEDGMENTS

This research was undertaken on the SAXS/WAXS beamline at the Australian Synchrotron, Victoria, Australia. Clive Bardell built some of the testing equipment. Sue Hallas of Nelson assisted with editing the manuscript.

REFERENCES

(1) Badylak, S. F.; Freytes, D. O.; Gilbert, T. W. Extracellular matrix as a biological scaffold material: Structure and function. *Acta Biomater.* **2009**, *5* (1), 1−13.

(2) Shevchenko, R. V.; James, S. L.; James, S. E. A review of tissue-engineered skin bioconstructs available for skin reconstruction. *J. R. Soc., Interface* **2010**, *7* (43), 229−258.

(3) Supp, D. M.; Boyce, S. T. Engineered skin substitutes: Practices and potentials. *Clinics in Dermatology* **2005**, *23* (4), 403−412.

(4) Cornwell, K. G.; Landsman, A.; James, K. S. Extracellular Matrix Biomaterials for Soft Tissue Repair. *Clinics in Podiatric Medicine and Surgery* **2009**, *26* (4), 507−523.

(5) Mohsina, A.; Kumar, N.; Sharma, A. K.; Mishra, B.; Mathew, D. D.; Remya, V.; Shrivastava, S.; Negi, M.; Kritaniya, D.; Mahan, P. T.; Maiti, S. K.; Singh, K. P. Bioengineered acellular dermal matrices for the repair of abdominal wall defects in rats. *Hernia* **2015**, *19* (2), 219−229.

(6) Winters, Z. E.; Colwell, A. S. Role of acellular dermal matrix-assisted implants in breast reconstruction. *Br. J. Surg.* **2014**, *101* (5), 444−445.

(7) Derwin, K. A.; Badylak, S. F.; Steinmann, S. P.; Iannotti, J. P. Extracellular matrix scaffold devices for rotator cuff repair. *Journal of Shoulder and Elbow Surgery* **2010**, *19* (3), 467−476.

(8) Lee, D. K. A preliminary study on the effects of acellular tissue graft augmentation in acute Achilles tendon ruptures. *J. Foot Ankle Surg.* **2008**, *47* (1), 8−12.

(9) MacNeil, S. Progress and opportunities for tissue-engineered skin. *Nature* **2007**, *445* (7130), 874−880.

(10) Lutolf, M. P.; Hubbell, J. A. Synthetic biomaterials as instructive extracellular microenvironments for morphogenesis in tissue engineering. *Nat. Biotechnol.* **2005**, *23* (1), 47−55.

(11) Blackwood, K. A.; McKean, R.; Canton, I.; Freeman, C. O.; Franklin, K. L.; Cole, D.; Brook, I.; Farthing, P.; Rimmer, S.; Haycock, J. W.; Ryan, A. J.; MacNeil, S. Development of biodegradable electrospun scaffolds for dermal replacement. *Biomaterials* **2008**, *29* (21), 3091−3104.

(12) Chen, X.; Qi, Y. Y.; Wang, L. L.; Yin, Z.; Yin, G. L.; Zou, X. H.; Ouyang, H. W. Ligament regeneration using a knitted silk scaffold combined with collagen matrix. *Biomaterials* **2008**, *29* (27), 3683−3692.

(13) Lun, S.; Irvine, S. M.; Johnson, K. D.; Fisher, N. J.; Floden, E. W.; Negron, L.; Dempsey, S. G.; McLaughlin, R. J.; Vasudevamurthy, M.; Ward, B. R.; May, B. C. H. A functional extracellular matrix biomaterial derived from ovine forestomach. *Biomaterials* **2010**, *31* (16), 4517−4529.

(14) Chen, R. N.; Ho, H. O.; Tsai, Y. T.; Sheu, M. T. Process development of an acellular dermal matrix (ADM) for biomedical applications. *Biomaterials* **2004**, *25* (13), 2679−2686.

(15) Bondioli, E.; Fini, M.; Veronesi, F.; Giavaresi, G.; Tschon, M.; Cenacchi, G.; Cerasoli, S.; Giardino, R.; Melandri, D. Development and evaluation of a decellularized membrane from human dermis. *J. Tissue Eng. Regener. Med.* **2014**, *8* (4), 325−336.

(16) Thomas, L. V.; Lekshmi, V.; Nair, P. D. Tissue engineered vascular grafts - Preclinical aspects. *Int. J. Cardiol.* **2013**, *167* (4), 1091−1100.

(17) Parekh, A.; Mantle, B.; Banks, J.; Swarts, J. D.; Badylak, S. F.; Dohar, J. E.; Hebda, P. A. Repair of the Tympanic Membrane with Urinary Bladder Matrix. *Laryngoscope* **2009**, *119* (6), 1206−1213.

(18) Brown, A. L.; Farhat, W.; Merguerian, P. A.; Wilson, G. J.; Khoury, A. E.; Woodhouse, K. A. 22 Week assessment of bladder acellular matrix as a bladder augmentation material in a porcine model. *Biomaterials* **2002**, *23* (10), 2179−2190.

(19) Lantz, G. C.; Badylak, S. F.; Coffey, A. C.; Geddes, L. A.; Blevins, W. E. Small intestinal submucosa as a small-diameter arterial graft in the dog. *J. Invest. Surg.* **1990**, *3* (3), 217−27.

(20) Mulder, G.; Lee, D. K. A Retrospective Clinical Review of Extracellular Matrices for Tissue Reconstruction: Equine Pericardium as a Biological Covering To Assist With Wound Closure. *Wounds-Compend. Clin. Res. Pract.* **2009**, *21* (9), 254−261.

(21) Lee, C. H.; Singla, A.; Lee, Y. Biomedical applications of collagen. *Int. J. Pharm.* **2001**, *221* (1−2), 1−22.

(22) Wells, H. C.; Sizeland, K. H.; Kayed, H. R.; Kirby, N.; Hawley, A.; Mudie, S. T.; Haverkamp, R. G. Poisson's ratio of collagen fibrils measured by SAXS of strained bovine pericardium. *J. Appl. Phys.* **2015**, *117* (4), 044701.

(23) Yang, W.; Sherman, V. R.; Gludovatz, B.; Schaible, E.; Stewart, P.; Ritchie, R. O.; Meyers, M. A. On the tear resistance of skin. *Nat. Commun.* **2015**, *6*, 6649.

(24) Loh, Q. L.; Choong, C. Three-Dimensional Scaffolds for Tissue Engineering Applications: Role of Porosity and Pore Size. *Tissue Eng., Part B* **2013**, *19* (6), 485−502.

(25) O'Brien, F. J. Biomaterials & scaffolds for tissue engineering. *Mater. Today* **2011**, *14* (3), 88−95.

(26) Wells, H. C.; Sizeland, K. H.; Kirby, N.; Hawley, A.; Mudie, S.; Haverkamp, R. G. Collagen Fibril Structure and Strength in Acellular Dermal Matrix Materials of Bovine, Porcine, and Human Origin. *ACS Biomater. Sci. Eng.* **2015**, *1* (10), 1026−1038.

(27) Floden, E. W.; Malak, S.; Basil-Jones, M. M.; Negron, L.; Fisher, J. N.; Lun, S.; Dempsey, S. G.; Haverkamp, R. G.; Ward, B. R.; May, B. C. H. Biophysical characterization of ovine forestomach extracellular matrix biomaterials. *J. Biomed. Mater. Res., Part B* **2011**, *96B* (1), 67−75.

(28) Zhang, J.; Wang, G. Y.; Xiao, Y. P.; Fan, L. Y.; Wang, Q. The biomechanical behavior and host response to porcine-derived small intestine submucosa, pericardium and dermal matrix acellular grafts in a rat abdominal defect model. *Biomaterials* **2011**, *32* (29), 7086−7095.

(29) Ge, L. P.; Zheng, S. Q.; Wei, H. Comparison of histological structure and biocompatibility between human acellular dermal matrix (ADM) and porcine ADM. *Burns* **2009**, *35* (1), 46−50.

(30) Sturrock, E. J.; Boote, C.; Attenburrow, G. E.; Meek, K. M. The effect of the biaxial stretching of leather on fibre orientation and tensile modulus. *J. Mater. Sci.* **2004**, *39*, 2481−2486.

DOI: 10.1021/acsbiomaterials.7b00588
ACS Biomater. Sci. Eng. XXXX, XXX, XXX−XXX

(31) Basil-Jones, M. M.; Edmonds, R. L.; Allsop, T. F.; Cooper, S. M.; Holmes, G.; Norris, G. E.; Cookson, D. J.; Kirby, N.; Haverkamp, R. G. Leather structure determination by small angle X-ray scattering (SAXS): Cross sections of ovine and bovine leather. *J. Agric. Food Chem.* **2010**, *58* (9), 5286−5291.
(32) Liao, J.; Yang, L.; Grashow, J.; Sacks, M. S. Molecular orientation of collagen in intact planar connective tissues under biaxial stretch. *Acta Biomater.* **2005**, *1* (1), 45−54.
(33) Sasaki, N.; Odajima, S. Stress-strain curve and youngs modulus of a collagen molecule as determined by the x-ray diffaction technique. *J. Biomech.* **1996**, *29* (5), 655−658.
(34) Kronick, P. L.; Buechler, P. R. Fiber orientation in calfskin by laser-light scattering or X-ray-diffraction and quantitative relation to mechanical-properties. *J. Am. Leather Chem. Assoc.* **1986**, *81* (7), 221−230.
(35) Basil-Jones, M. M.; Edmonds, R. L.; Cooper, S. M.; Haverkamp, R. G. Collagen fibril orientation in ovine and bovine leather affects strength: A small angle X-ray scattering (SAXS) study. *J. Agric. Food Chem.* **2011**, *59* (18), 9972−9979.
(36) Basil-Jones, M. M.; Edmonds, R. L.; Norris, G. E.; Haverkamp, R. G. Collagen fibril alignment and deformation during tensile strain of leather: a small-angle X-ray scattering study. *J. Agric. Food Chem.* **2012**, *60* (5), 1201−1208.
(37) Sizeland, K. H.; Basil-Jones, M. M.; Edmonds, R. L.; Cooper, S. M.; Kirby, N.; Hawley, A.; Haverkamp, R. G. Collagen Orientation and Leather Strength for Selected Mammals. *J. Agric. Food Chem.* **2013**, *61* (4), 887−892.
(38) Sizeland, K. H.; Edmonds, R. L.; Basil -Jones, M. M.; Kirby, N.; Hawley, A.; Mudie, S.; Haverkamp, R. G. Changes to collagen structure during leather processing. *J. Agric. Food Chem.* **2015**, *63* (9), 2499−2505.
(39) Sizeland, K. H.; Wells, H. C.; Norris, G. E.; Edmonds, R. L.; Kirby, N.; Hawley, A.; Mudie, S.; Haverkamp, R. G. Collagen D-spacing and the effect of fat liquor addition. *J. Am. Leather Chem. Assoc.* **2015**, *110* (3), 66−71.
(40) Sizeland, K. H.; Holmes, G.; Edmonds, R. L.; Kirby, N.; Hawley, A.; Mudie, S. T.; Haverkamp, R. G. Fatliquor effects on collagen fibril orientation and d-spacing in leather during tensile strain. *J. Am. Leather Chem. Assoc.* **2015**, *110* (11), 355−362.
(41) Chan, Y.; Cox, G. M.; Haverkamp, R. G.; Hill, J. M. Mechanical model for a collagen fibril pair in extracellular matrix. *Eur. Biophys. J.* **2009**, *38* (4), 487−493.

DOI: 10.1021/acsbiomaterials.7b00588
ACS Biomater. Sci. Eng. XXXX, XXX, XXX−XXX